Electronic Supplementary Material (ESI) for Journal of Materials Chemistry A.


# Defects and disorder in apatite-type silicate oxide ion conductors: implications for conductivity

Chloe A. Fuller,[a] Matthias J. Gutmann[b], Chris D. Ling[c], Chun-Hai Wang[c], P. Shiv Halasyamani[d], Ivana Radosavljevic Evans[a,*], and John S. O. Evans [a,*]

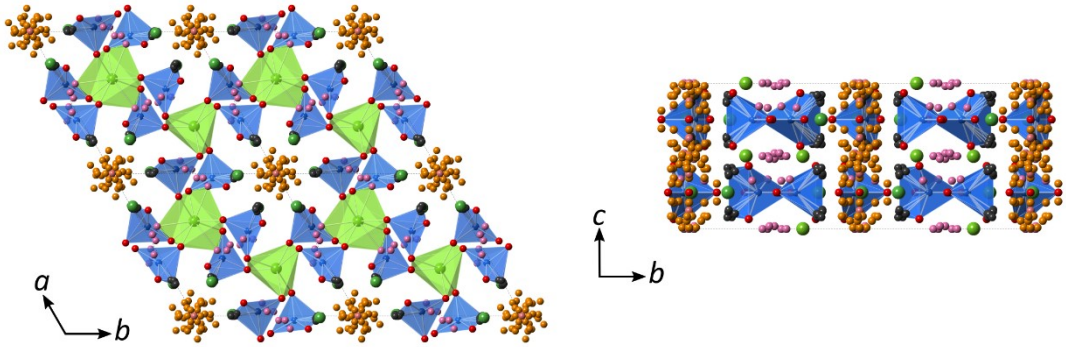


*Figure S1. Illustrations of the interstitial sites that have been proposed in $La_{9.33+x}(SiO_4)_6O_{26+1.5x}$ including symmetry equivalents. Three main areas can be identified: near the $SiO_4$ groups coloured grey, between two $SiO_4$ groups coloured pink and within the O4 channel coloured orange.*

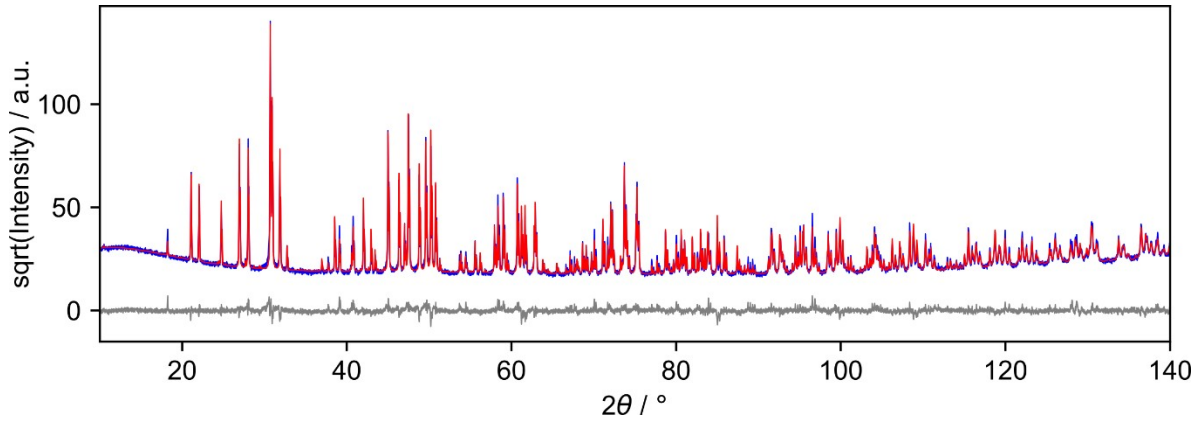


*Figure S2. Rietveld refinement of crushed crystals of $La_{9.64}Si_{5.77}O_{26}$. $R_{wp}$ = 8.898%, GOF = 2.27.*

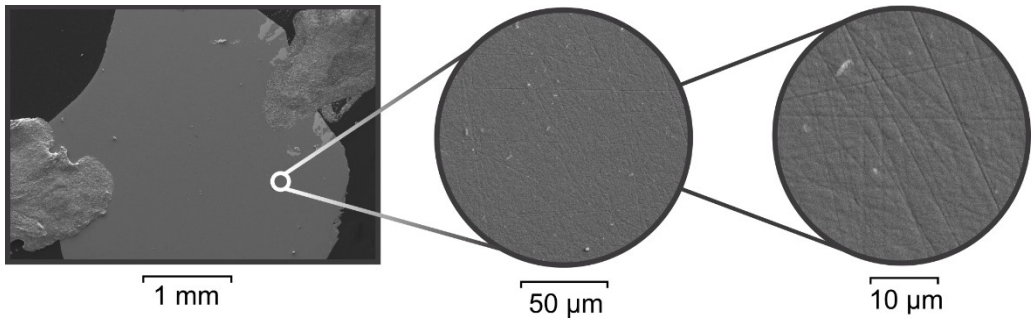


*Figure S3. SEM micrographs of the polished LSO crystal. The gold paste used to prevent charge build-up is visible in the top right and bottom left corners. The micrographs in circles show progressively smaller length scales to show the homogeneity of the crystal. The lighter-coloured flecks result from the carbon coating and the straight lines from the polishing treatment.*

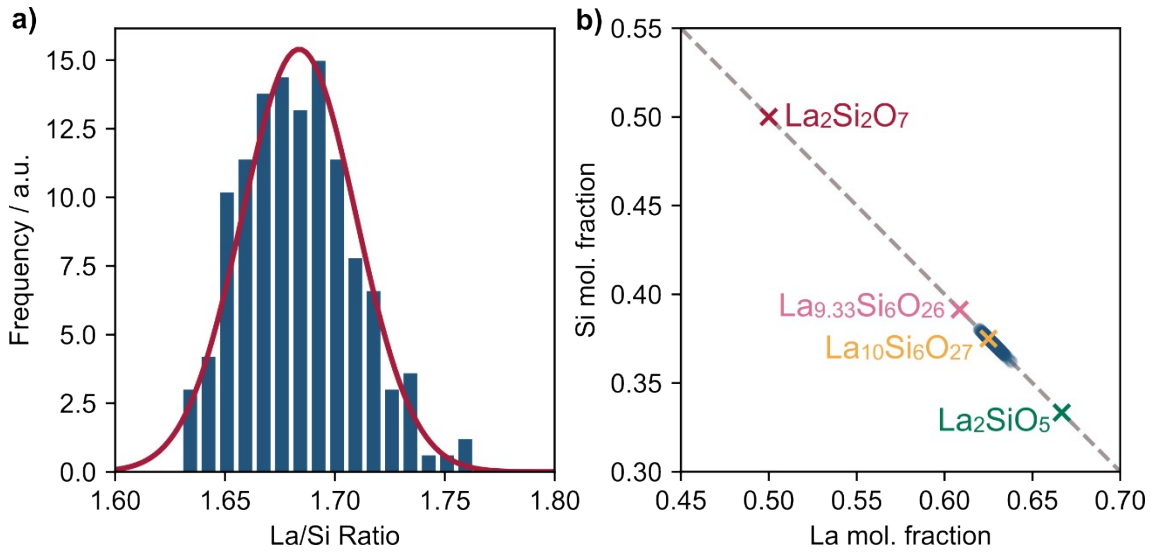


*Figure S4. a) A histogram of the La:Si ratios measured by SEM-EDX, using 225 spectra from 5 different sites on a polished crystal of LSO, fitted with the red gaussian distribution. b) Compounds related to LSO expressed as Si and La mole fractions. The experimental mole fractions of LSO calculated from the histogram in a) are shown with blue shading. The nominal mole fractions of related compositions are marked on the graph for comparison.*

The Gaussian fit to the histogram gives a mean La/Si ratio of 1.684(2) and a standard deviation of 0.026. This corresponds to $La_{9.67}Si_{5.74}O_{26}$, when normalised to $O_{26}$. To give an idea of the precision of this EDX technique, one standard deviation away from the mean in either direction corresponds to ratios of 1.710 and 1.658, which give the compositions $La_{9.73}Si_{5.75}O_{26}$ and $La_{9.61}Si_{5.79}O_{26}$, respectively. There is an approximate <1% difference in the Si content between the latter two compositions.

## Specific gravity measurements

Due to the effects of buoyancy, crystals weigh less in ethanol than in air and the specific gravity can be calculated using

$$G_{crystal} = \frac{m_{air}}{m_{air} - m_{EtOH}} G_{EtOH}, \qquad \text{Eq. S1}$$

where $m$ is the mass and $G$ is the specific gravity (0.7893 g cm$^{-3}$ for ethanol at 20 °C). The density of the crystal is then $G_{crystal} \times \rho_{water}$, where $\rho_{water}$ is the density of water. A simple apparatus to allow density measurements was mounted on a 4-decimal-place balance, as described by Brandriss[1]. The experimental uncertainty was quantified by measuring the specific gravity of four materials with known density: quartz glass pieces, silicon wafers, and agate and zirconia milling balls; a summary of the standard measurements is given in Table S1. For quartz and silicon, the known density corresponds to the theoretical density, and for the milling balls, the density was measured using their mass and volume. For each material, between 6 and 15 different samples were measured. This confirmed the accuracy of the experiment and defined a typical standard deviation of 0.02 g cm$^{-3}$. The primary source of error is the precision of the balance, and scales as 1/mass of the crystal. Test measurements determined that the crystal must weigh more than 0.05 g to produce a meaningful measured density value. The specific gravities of four different pieces of the LSO (with masses 0.2878, 0.1660, 0.0897 and 0.0755 g) were each measured 20 times to provide an average density for the crystals.

*Table S1. Comparison between the measured and known densities standard samples.*

| **Standard** | **$\rho_{known}$ / g cm$^{-3}$** | **$\rho_{measured}$ / g cm$^{-3}$** |
|---|---|---|
| Agate bead | 2.60 | 2.585(3) |
| $ZrO_2$ bead | 6.05 | 6.066(3) |
| Si wafer | 2.33 | 2.33(1) |
| Quartz glass | 2.20 | 2.191(4) |

| Point | La content | Density / g cm$^{-3}$ | Si content | O content |
|---|---|---|---|---|
| 1 | 9.615 | 5.410 | 5.789 | 26 |
| 2 | 9.640 | 5.418 | 5.770 | 26 |
| 3 | 9.675 | 5.430 | 5.744 | 26 |
| 4 | 9.651 | 5.430 | 5.820 | 26.12 |
| 5 | 9.642 | 5.410 | 5.726 | 25.91 |

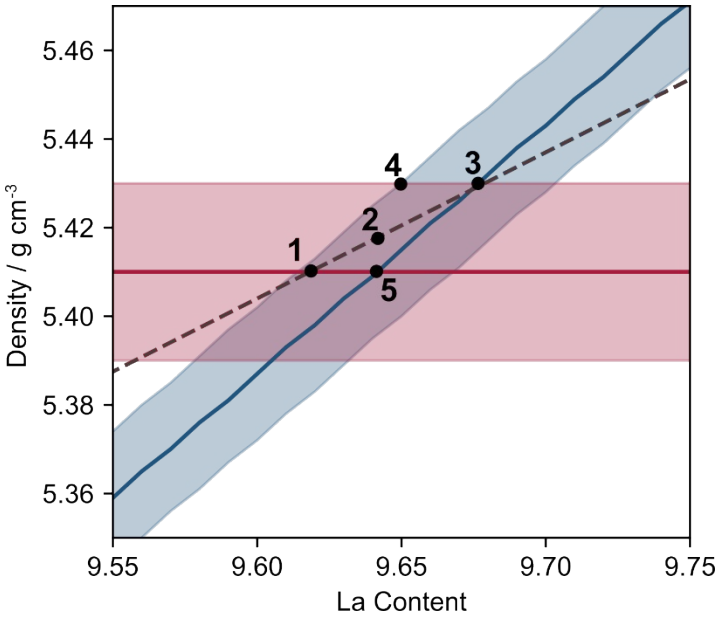


*Figure S5. Zoom of Figure 2 in the main text showing the estimate of the final composition (point 2) and the upper and lower bounds of composition assuming oxygen stoichiometry (points 1 and 2). Shaded regions represent one standard*

*deviation away from the mean for the measured density (pink) and calculated density using $La_xSi_{x/1.684}O_{[3x+4(x/1.684)]/2}$. The dotted line indicates oxygen stoichiometric compositions, i.e. $La_xSi_{(52-3x)/4}O_{26}$.*

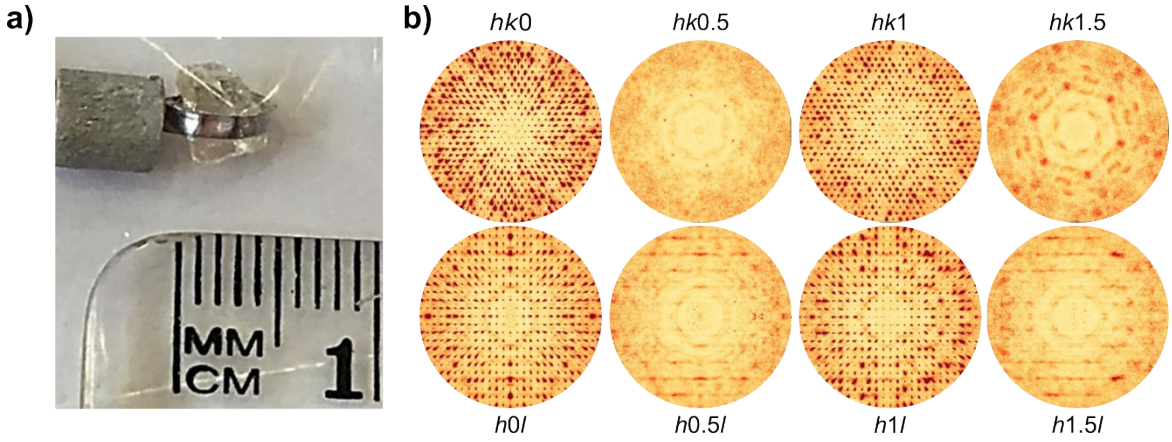


*Figure S6. a) The crystal used for neutron diffraction measurement and b) example diffraction planes reconstructed from the neutron diffraction data collected on LSO at 40 K. Significant diffuse scatter is seen between the Bragg peaks.*

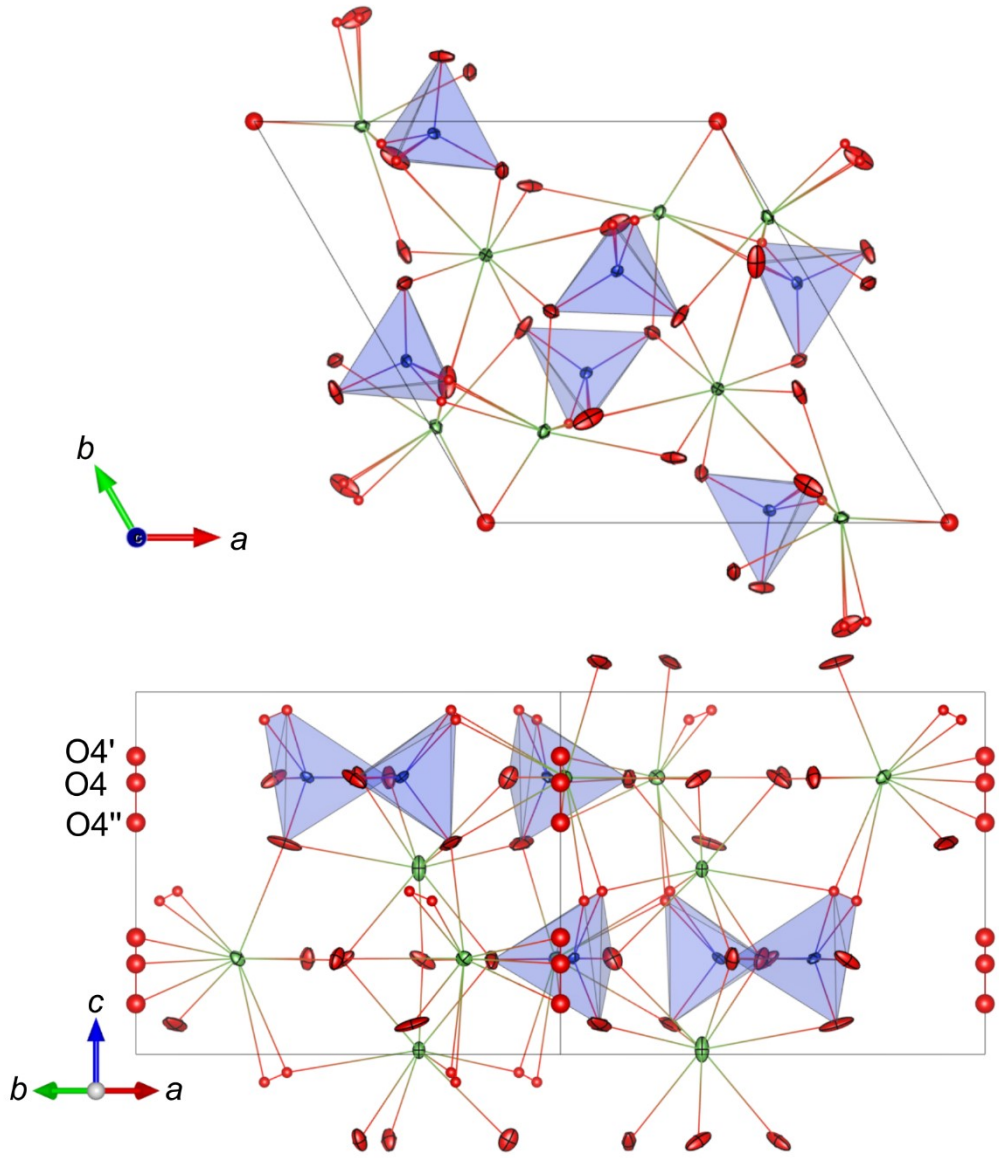


*Figure S7. Final refined room temperature structure with ellipsoids drawn at 50% probability.*

*Table S2. Summary of single crystal neutron refinements for LSO at 40 and 295 K.*

| **Temperature** | **40K** | **295K** |
|---|---|---|
| Space group | $P6_3$ | $P6_3$ |
| *a* / Å | 9.7027(17) | 9.7133(17) |
| *c* / Å | 7.1793(16) | 7.1843(18) |
| *V* / Å$^3$ | 585.33(16) | 587.01(17) |
| # Reflections | | |
| all | 20874 | 10449 |
| Observed (>3$\sigma$) | 15339 | 7385 |
| Excluded ($\lvert F_{obs}-F_{calc}\rvert$ > 10$\sigma$) | 779 | 366 |
| *R* / % | 7.72 | 6.92 |
| *wR* / % | 6.81 | 6.23 |

*Table S3. Refined structural parameters for $La_{9.64}Si_{5.77}O_{26}$.*

| Site | | Occ. | x | y | z | $U_{iso}$ / Å² | $U_{11}$ / Å² | $U_{22}$ / Å² | $U_{33}$ / Å² | $U_{12}$ / Å² | $U_{23}$ / Å² | $U_{13}$ / Å² |
|---|---|---|---|---|---|---|---|---|---|---|---|---|
| **295K** | | | | | | | | | | | | |
| La1_1 | 2*b* | 0.841(6) | 0.3333 | 0.6667 | 0.0118(2) | 0.0112(5) | 0.0106(7) | 0.0106(7) | 0.0123(6) | 0.0053(4) | 0 | 0 |
| La1_2 | 2*b* | 0.979(6) | 0.6667 | 0.3333 | 0.0140(1) | 0.0133(5) | 0.0054(6) | 0.0054(6) | 0.0292(8) | 0.0027(3) | 0 | 0 |
| La2 | 6*c* | 1 | 0.22725(5) | -0.01205(4) | 0.2639(2) | 0.0086(1) | 0.0010(1) | 0.0062(1) | 0.0092(1) | 0.0037(1) | -0.0001(4) | 0.0007(4) |
| Si1 | 6*c* | 0.9617 | 0.40306(8) | 0.37292(9) | 0.2652(3) | 0.0047(2) | 0.0053(3) | 0.0051(3) | 0.0044(1) | 0.0037(2) | -0.0017(7) | -0.0030(7) |
| O1 | 6*c* | 1 | 0.32472(9) | 0.48604(9) | 0.2601(3) | 0.0170(3) | 0.0246(4) | 0.0222(4) | 0.0152(2) | 0.0199(3) | 0.0109(5) | 0.0123(5) |
| O2 | 6*c* | 1 | 0.59592(7) | 0.47326(7) | 0.2585(3) | 0.0144(2) | 0.0091(3) | 0.0096(3) | 0.0208(2) | 0.0019(2) | -0.0006(7) | 0.0048(7) |
| O3_1 | 6*c* | 1 | 0.3495(3) | 0.2579(2) | 0.0773(2) | 0.0238(6) | 0.0487(11) | 0.0209(6) | 0.0089(3) | 0.0228(7) | -0.0142(4) | -0.0088(3) |
| O3_2 | 6*c* | 0.312(4) | 0.3024(4) | 0.2469(4) | 0.4178(4) | 0.0053(2) | | | | | | |
| O3_2' | 6*c* | 0.688(4) | 0.3559(2) | 0.2581(2) | 0.4446(2) | 0.0053(2) | | | | | | |
| O4 | 2*a* | 0.4577(4) | 0 | 0 | 0.2504(5) | 0.0149(5) | | | | | | |
| O4' | 2*a* | 0.349(4) | 0 | 0 | 0.3218(7) | 0.0149(5) | | | | | | |
| O4" | 2*a* | 0.193(4) | 0 | 0 | 0.1408(10) | 0.0149(5) | | | | | | |
| **40K** | | | | | | | | | | | | |
| La1_1 | 2*b* | 0.856(3) | 0.3333 | 0.6667 | 0.0004(2) | 0.0079(3) | 0.0063(3) | 0.0063(3) | 0.0110(4) | 0.0031(2) | 0 | 0 |
| La1_2 | 2*b* | 0.964(3) | 0.6667 | 0.3333 | 0.0030(1) | 0.0098(2) | 0.0027(3) | 0.0027(3) | 0.0241(5) | 0.0013(1) | 0 | 0 |
| La2 | 6*c* | 1 | 0.22732(3) | -0.01214(3) | 0.2500(2) | 0.00628(8) | 0.00298(8) | 0.00533(6) | 0.00556(6) | 0.00145(7) | 0.0009(2) | -0.0009(2) |
| Si1 | 6*c* | 0.9617 | 0.40311(5) | 0.37280(5) | 0.2496(3) | 0.0036(1) | 0.0052(1) | 0.0040(1) | 0.0027(1) | 0.0031(1) | 0.0001(4) | 0.0006(4) |
| O1 | 6*c* | 1 | 0.32482(6) | 0.48629(6) | 0.2527(3) | 0.0129(1) | 0.0183(2) | 0.0189(2) | 0.0109(1) | 0.0163(2) | -0.0092(3) | -0.0108(3) |
| O2 | 6*c* | 1 | 0.59642(5) | 0.47338(5) | 0.2452(3) | 0.0096(1) | 0.0064(1) | 0.0056(1) | 0.0139(1) | 0.0009(1) | -0.0017(3) | 0.0007(4) |
| O3_1 | 6*c* | 1 | 0.3525(2) | 0.2582(1) | 0.0667(2) | 0.0175(3) | 0.0373(6) | 0.0173(3) | 0.0044(1) | 0.0186(3) | -0.0107(2) | -0.0069(1) |
| O3_2 | 6*c* | 0.306(4) | 0.3024(2) | 0.2463(2) | 0.4124(3) | 0.0050(3) | | | | | | |
| O3_2' | 6*c* | 0.694(4) | 0.3544(1) | 0.2573(2) | 0.4347(3) | 0.0050(2) | | | | | | |
| O4 0 | 2*a* | 1 | 0 | 0 | 0.2399(13) | 0.0674(9) | 0.0099(3) | 0.0099(3) | 0.182(3) | 0.0050(1) | 0 | 0 |

*Table S4. Refined bond lengths for La and Si polyhedra at 295 and 40 K. The distance between O3_2 and O3_2' is 0.50 Å at both temperatures, and at 295 K, the distances O4–O4', O4–O4'' and O4'–O4'' are 0.51, 0.79 and 1.30 Å, respectively.*

| 295K | | 40K | |
|---|---|---|---|
| **Bond** | **Bond Length / Å** | **Bond** | **Bond Length / Å** |
| La1_1 – O1 (x3) | 2.4737 | La1_1 – O1 (x3) | 2.5002 |
| La1_1 – O2 (x3) | 2.5343 | La1_1 – O2 (x3) | 2.5590 |
| La1_1 – O3_2' (x3) | 2.7751 | La1_1 – O3_2' (x3) | 2.7753 |
| La1_1 – O3_2 (x3) | 3.2622 | La1_1 – O3_2 (x3) | 3.2694 |
| La1_2 – O1 (x3) | 2.5035 | La1_2 – O1 (x3) | 2.4720 |
| La1_2 – O2 (x3) | 2.5470 | La1_2 – O2 (x3) | 2.5107 |
| La1_2 – O3_1 (x3) | 2.8023 | La1_2 – O3_1 (x3) | 2.7969 |
| La2 – O4 | 2.2701 | La2 – O4 | 2.2693 |
| La2 – O4' | 2.3059 | La2 – O3_2' | 2.4749 |
| La2 – O4'' | 2.4344 | La2 – O3_1 | 2.4769 |

| | | | |
|---|---|---|---|
| La2 – O3_2’ | 2.4713 | La2 – O3_2 | 2.4966 |
| La2 – O3_1 | 2.4857 | La2 – O3_2 | 2.5154 |
| La2 – O3_2 | 2.5030 | La2 – O2 | 2.5191 |
| La2 – O3_2 | 2.5124 | La2 – O3_2’ | 2.6250 |
| La2 – O2 | 2.5221 | La2 – O3_1 | 2.6271 |
| La2 – O3_1 | 2.6305 | La2 – O1 | 2.7703 |
| La2 – O3_2’ | 2.6328 | Si – O3_2 | 1.6122 |
| La2 – O1 | 2.7729 | Si – O1 | 1.6207 |
| Si – O3_2 | 1.6022 | Si – O2 | 1.6251 |
| Si – O1 | 1.6197 | Si – O3_1 | 1.6294 |
| Si – O2 | 1.6231 | Si – O3_2’ | 1.6480 |
| Si – O3_1 | 1.6321 | | |
| Si – O3_2’ | 1.6443 | | |

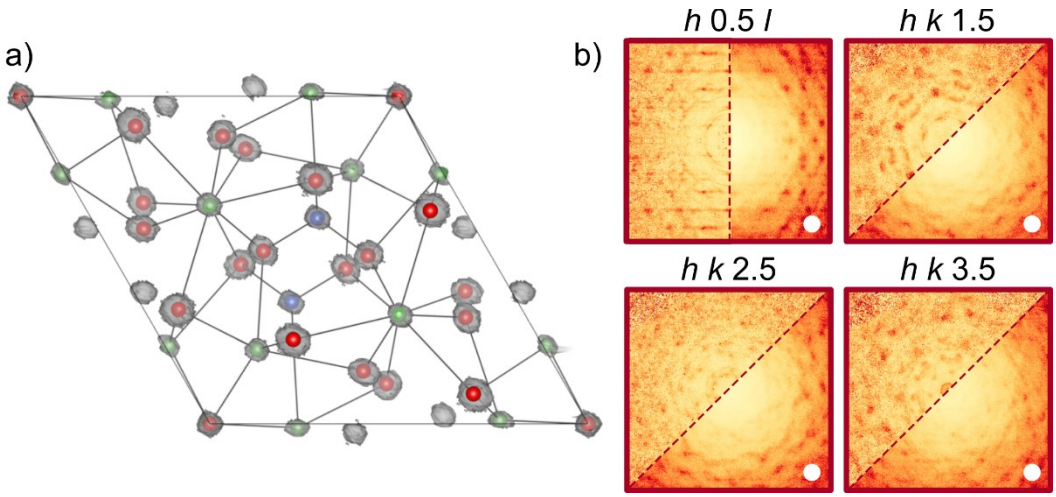


*Figure S8. a) The large box model used to simulate diffuse scattering folded back down into a single unit cell. The green, blue and red spheres shows the average positions of La, Si and O, respectively, and the grey clouds encompass the positions of all the atoms in the supercell. b) Selected experimental and simulated diffuse scattering h k l sections. Calculated patterns are indicated with a white circle and the dividing line between calculated and experimental patterns is shown by a red dashed line. Intensities of the calculated patterns are arbitrary and are coloured to match the experimental patterns.*

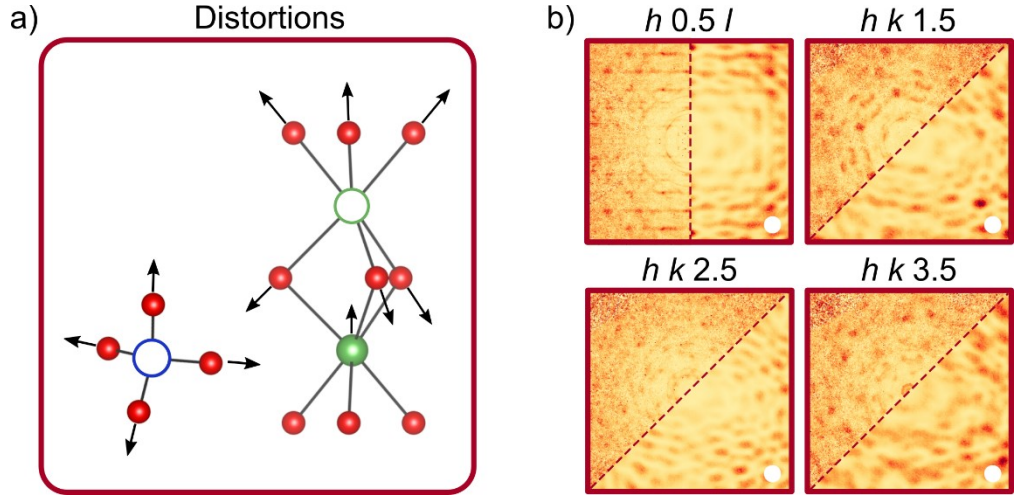


*Figure S9. a) Breathing distortions around Si (blue circle) and La vacancies (green circle); note that the arrows are not to scale. b) The resulting calculated diffuse scattering and corresponding experimental sections.*

## Modelling O4 displacement correlations

O4 atoms were distributed across the three sites identified from the RT refinement, as shown in Figure S10a, with the central atom at fractional coordinates (0, 0, 0.25) and the other two shifted up or down along the *c*-axis to (0, 0, 0.35) and (0, 0, 0.15). The occupancies of these three sites from the structure refinement suggest that the central position is occupied ~50% of the time. For simplicity in this model, the remaining 50% of atoms was distributed over the upper and lower sites equally.

An Ising-like energy function can be employed to allow different correlations in the O4 positions to be created. The three sites were assigned a pseudo-spin value of -1, 0 and 1 for lower, central and upper sites, respectively. A Monte Carlo ordering algorithm was written to swap O4 atoms with different spins and calculate the energies of the two configurations according to

$$E_i = \sum_{j=1}^{n} - k_{ij}\sigma_i\sigma_j \qquad \text{Eq. S2}$$

where $E_i$ is the energy of atom *i*, $k_{ij}$ is the force constant between O4 atom *i* and its O4 neighbour *j*, $\sigma_i$ is the assigned spin of atom *i* and *n* is the number of neighbours of atom *i*. To clarify, for this section of the modelling, the neighbours of atom *i* refer to its neighbouring O4 atoms even though they are nominally non-bonded. Each O4 has eight neighbours: six in the *ab*-plane, one above it, and one below. The starting force constant matrix was defined arbitrarily to make like spins have a weak interaction, opposite spins have a strong interaction, and spins of 0 to have no interactions. This definition was found by trial and error to give the desired ordering patterns.

A correlation between spins can be used to quantify the ordering patterns produced by the algorithm. After each MC cycle, the correlation is calculated by

$$\text{corr} = \frac{\sum \sigma_i\sigma_j}{n} \qquad \text{Eq. S3}$$

For like spins, $\sigma_i\sigma_j$ = 1, so if atom *i* is completely surrounded by like spins, corr = 1. If all the spins are opposing, corr = -1. A correlation can, therefore, be specified to define the type of ordering desired. The force constants are then scaled by the difference between the calculated and desired correlation value at the end of each MC cycle. Using this method, the O4 positions can be correlated separately in the *ab*-plane and along the *c*-axis with the sum in Equation S2 running over the two neighbours above and below the plane, or the six neighbours in the *ab*-plane, respectively. Example configurations are given in Figures S10b and S10c, where yellow, red and blue spheres represent O4 atoms in the lower, central and upper positions from Figure S10a. The configuration in S10b has a correlation of 0.35 parallel to the *c*-axis and 0.0 in the *ab*-plane, so like spins are clustered along the *c*-axis and are randomly distributed in the *ab*-plane. Note that a correlation significantly higher than 0.35 is not possible in this model as the three different spins necessitate that some neighbour interactions are not between like spins, so the overall correlation decreases. In the final model, these correlations translate to O4 atoms with the same vertical displacement being clustered together along *c*, approximating the correlated displacements that would result from electrostatics in a real material. The corresponding anti-correlation, where adjacent O4s prefer to be displaced in opposite directions, would model the effects of elastic strain in the LSO crystal.

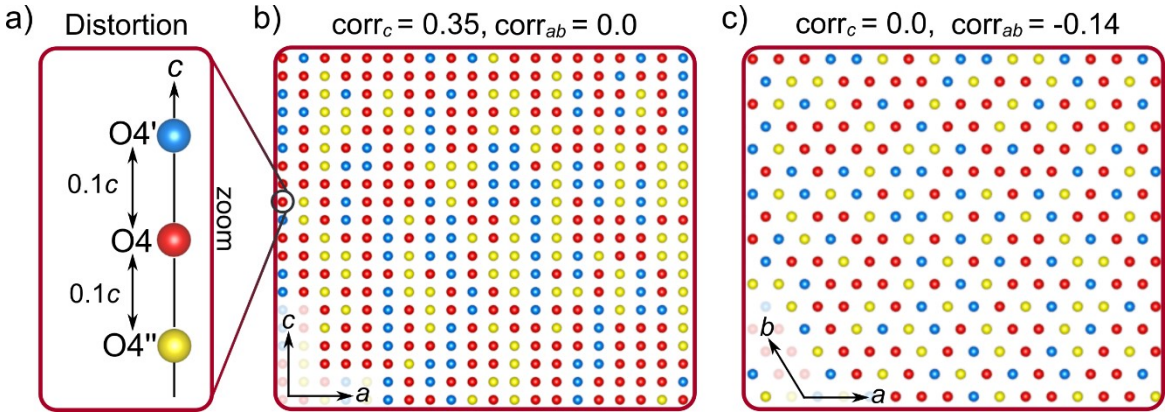


*Figure S10. a) Modelling of the disorder on the O4 site. For each O4 in the supercell, the atom was place on one of the positions indicated by the coloured spheres with 50% on the central position and 25% on the other two. b, c) Example configurations of the supercell showing only the O4 atoms to show the different ordering patterns produced. The colours correspond to the positions in a.*

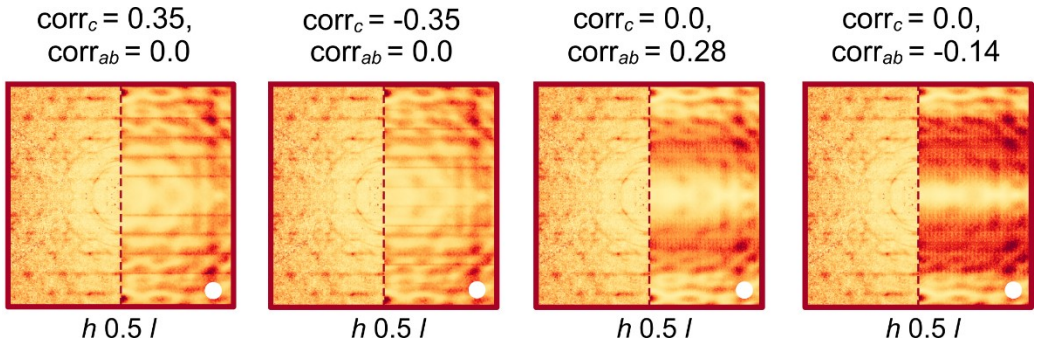


*Figure S11. Diffuse scattering patterns produced by different correlations of O4 positions and the corresponding experimental patterns.*

1 E. Brandriss, Mark, *J. Geosci. Educ.*, 2010, **58**, 155–165.